Spin-resolved off-specular neutron scattering maps from magnetic multilayers using a polarized ^{3}He gas spin filter

B. Nickel, A. Rühm,[a] W. Donner, J. Major, and H. Dosch
Max-Planck-Institut für Metallforschung, Heisenbergstrasse 1, D-70569 Stuttgart, Germany
and Institut für Theoretische und Angewandte Physik, Universität Stuttgart, D-70569 Stuttgart, Germany

A. Schreyer and H. Zabel
Institut für Experimentalphysik/Festkörperphysik, Ruhr-Universität Bochum, D-44780 Bochum, Germany

H. Humblot
Institute Laue–Langevin, 6, rue Jules Horowitz, BP 156, F-38042 Grenoble Cedex 9, France

(Received 18 April 2000; accepted for publication 3 October 2000)

We report on the application of the polarized ^{3}He gas spin filter technique for the measurement of spin-polarized diffuse neutron reflectivity with spin analysis. The spin filter together with a one-dimensional position-sensitive detector enables the simultaneous investigation of sections in reciprocal space while exploiting spin sensitivity. An example of diffuse neutron scattering from a Fe/Cr superlattice demonstrates the potential of the method. In addition we present a first step towards the interpretation of diffuse scattering from magnetic multilayers by exploiting the supermatrix formalism. © *2001 American Institute of Physics.* [DOI: 10.1063/1.1328403]

I. INTRODUCTION

The magnetic structure of thin magnetic superlattices has attracted much attention in the past few years because of their novel and widely tunable interlayer magnetic coupling phenomena and the associated magneto-transport properties.[1] Various experimental techniques have been devised to unravel the magnetic structure of these artificial nanostructures, among them polarized neutron reflectivity which provides detailed information about the laterally averaged magnetization profile across the multilayers.[2] In the last several years it became apparent that the magnetic roughness of the interfaces and the magnetic domains within the ferromagnetic layers [shown schematically in Fig. 1(a)] play an important role in understanding of the observed average magnetic interlayer coupling; furthermore, magnetic roughness and magnetic domains and in particular the spatial correlations between them seem to be crucial for the performance of such devices.[3] The microscopic characterization of such magnetic imperfections demands techniques which are, on the one hand, sensitive to local magnetic moments and their spatial distribution and, on the other hand, suited to study these real structures in buried layers and interfaces. We will show in this article that spin-resolved off-specular neutron scattering is able to tackle this task, if a proper experimental setup is employed.

Any diffraction pattern from imperfect magnetic multilayers can be divided into two contributions (see Fig. 1), the specular reflected intensity (characterized by inplane momentum transfer $q_\parallel = 0$) originating from the laterally averaged density profile and the off-specular diffuse scattering which is caused by all local deviations from the average profile. This off-specular scattering is detected as a broad diffuse background around the forward direction and exhibits a characteristic angular dependence which eventually reflects correlations present between the local imperfections. Thus, in order to ''reconstruct'' the microscopic details of magnetic roughness and of magnetic domains, it is mandatory to explore the small diffuse background in the entire reciprocal space within the first Brillouin zone. Figure 1(b) shows schematically the diffuse scattering profile associated with the real structure of Fig. 1(a) as a function of the inplane momentum transfer $q_\parallel$: The broad featureless component results from the local uncorrelated steps and kinks at the interfaces, and its inverse width is given by the inplane correlation length ξ_R which is assumed here to be microscopically small. The other component may be termed small angle scattering from magnetic domains of submicrometer size ξ_D. Correlations of roughness or domains between layers are observed by a characteristic modulation of this diffuse scattering as a function of the normal momentum transfer q_z (see, for example, Ref. 4).

Due to the small amount of local scattering centers in highly perfect multilayer systems, the magnetic off-specular diffuse scattering intensity is usually rather low and, if detectable at all, partially buried under the off-specular scattering contribution from the chemical roughness of the interfaces. X-ray scattering techniques appear at first to be more favorable than neutron scattering because of the availability of highly brilliant synchrotron sources which provide a large x-ray flux at the sample surface. Indeed, several experiments have recently been performed to explore the potential of magnetic off-specular x-ray scattering.[5–7] It turns out, however, that, despite the success of these experiments, magnetic off-specular x-ray scattering is hampered by the very low magnetic x-ray scattering cross section and the rather com-

[a]Present address: Advanced Photon Source, IMM-CAT, 9700 South Cass Avenue, Argonne, IL 60439-4832; electronic mail: adrian@slate.imm.aps.anl.gov

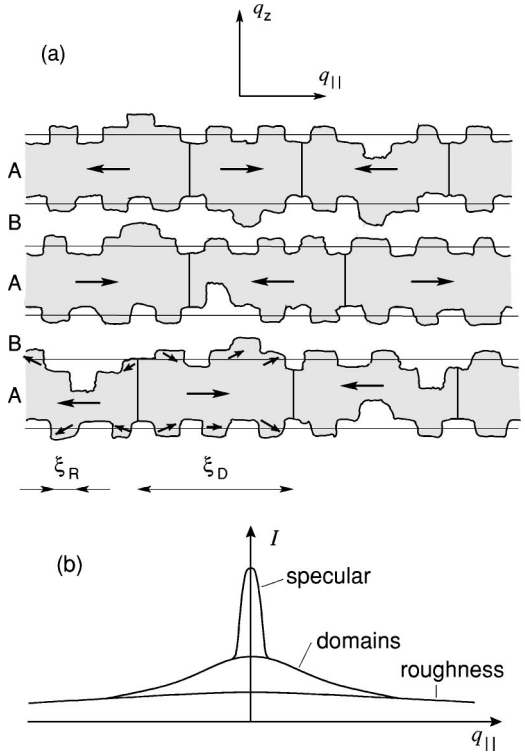

FIG. 1. (a) Sketch of an antiferromagnetically ordered magnetic multilayer exhibiting local imperfections and domains. (b) Diffraction pattern corresponding to (a).

plicated magnetic x-ray interaction potential which seems to prevent direct, quantitative access to the local correlations of the magnetic moments.

Off-specular diffuse neutron scattering would in fact avoid all the aforementioned problems associated with x rays, since it is governed by a rather simple scattering cross section with direct access to the spin–spin correlation function as was demonstrated recently for a single selected off-specular scan.[8] However, it generally suffers from the low brilliance of the available neutron sources, thus, the resulting very low scattering distribution within the first Brillouin zone can only be recorded within reasonable measuring times by using multidetection techniques. On the other hand, the magnetic diffuse scattering must be separated from the nuclear diffuse neutron scattering arising from chemical roughness of the interfaces by using polarized neutrons and applying a spin analysis of the scattered neutrons. In order to combine these two prerequisites, i.e., spin analysis of the scattered neutrons and use of multidetector systems, we propose to use a spin-filtering technique for scattered neutrons by means of a polarized ^{3}He gas which allows one to simultaneously analyze the polarization of each scattered neutron recorded in the multidetector system.

^{3}He spin filters have been developed, tested and improved since 1991,[9–11] and are or will soon be available at several neutron laboratories.[12–17] ^{3}He filters have already been successfully applied in experimental studies, e.g., on in-chain spin correlations in $YBa_2Cu_3O_{6+x}$ (Ref. 18) and on neutron optics *P*-violation effects,[19] as well as in paramagnetic scattering experiments on a $Fe_{0.77}Ni_{0.13}Mn_{0.07}C_{0.03}$ alloy.[20] Due to the extremely high degree of polarization that

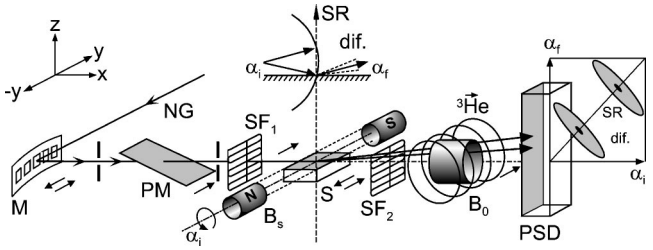

FIG. 2. Outline of the experimental setup. The neutrons are supplied by a neutron guide (NG) and diffracted by a monochromator (M). After passing a slit, they are polarized by a transmission mirror PM and may be flipped by a Mezei flipper SF_1. The sample S is placed in an external field B and can be inclined by an angle α_i. The reflected or scattered neutrons pass a second flipper SF_2 before entering the ^{3}He vessel placed in a homogeneous field B_0. PSD acquires the exit angle profiles containing the specular rod (SR) ($\alpha_i = \alpha_f$) together with the off-specular scattering.

can be achieved with ^{3}He filters, they have been proposed as a tool with which to test the electroweak standard model.[21] Application in neutron crosscorrelation spectroscopy has also been suggested.[22] Further applications of ^{3}He are described in Ref. 23. Very recently, these filters have been used for polarization analysis in (bulk) small-angle neutron scattering.[24] So far, ^{3}He filters have not yet been utilized for polarized neutron reflectometry or studies of magnetic multilayers like that presented in this article. It is expected, however, that the performance[25,26] and availability of these devices will improve in the near future. As indicated by the results of this article, they could then most effectively be used in polarized neutron reflectometry, especially in combination with one- and two-dimensional multidetection schemes.[24]

In this article we describe the first test of such a neutron scattering setup realized at the evanescent neutron wave diffractometer EVA which was equipped with a ^{3}He filter and a one-dimensional position sensitive detector. We discuss a pilot experiment performed on a Fe/Cr multilayer which is known to exhibit a peculiar noncollinear average magnetization profile.[27] We further show that the so-called supermatrix formalism,[28] recently developed to analyze polarized neutron reflectometry data, can be extended to rigorously and efficiently analyze the spin-resolved diffuse neutron scattering maps obtained in such an experiment.

II. EXPERIMENTAL DETAILS

Here in Sec. III we describe the essential features of the experimental setup and the sample preparation, thereby focusing on the performance of the ^{3}He filter.

A. Outline of the off-specular scattering setup

The off-specular neutron scattering experiments were performed at the evanescent neutron wave diffractometer EVA at the high flux reactor of the Institute Laue–Langevin in Grenoble. EVA is designed as a test instrument to explore the potential of surface and interface scattering using tunneling neutron waves (evanescent waves).[29,30] A sketch of the experimental setup is shown in Fig. 2. The instrument is supplied with neutrons of wavelength $\lambda = 5.5$ Å by a recently installed new horizontally focusing monochromator, which is

made of five pieces of highly oriented pyrolytic graphite (HOPG) crystals with an individual mosaic spread of 0.3° full width at half maximum (FWHM). The focal length is conveniently tunable by stepping motor controlled goniometer heads, and for reflectivity experiments the focal spot is at the sample position to maximize the flux at the sample surface. Furthermore, the reflected beam from the monochromator can be tilted vertically for experiments on liquid surfaces.[31]

The monochromatic beam is subsequently polarized in the y direction by means of a polarizing transmission mirror (PM) with a polarizing efficiency of $p_1 = 97\%$. Using downstream Mezei flipper SF_1 (flipping efficiency $f_1 = 97.5\%$) the polarization of the beam can be reversed into the $-y$ direction. At the sample position a magnetic field B between 50 and 400 mT can be applied parallel to the sample surface (y direction). The specularly reflected and off-specularly scattered neutrons are simultaneously recorded by a linear position-sensitive wire counter providing exit-angle scans (α_f scans; see Fig. 2). For analysis of the spin state of each recorded neutron in the detector a polarized ^{3}He gas neutron spin filter is installed between the sample and the detector (details of the ^{3}He filter will be given below). In the spin-resolved operation mode, scans of the incidence angle α_i are performed and four α_f profiles are recorded at each α_i position, one for each of the four scattering cross sections $++$, $--$, $+-$ and $-+$, where ''+'' refers to the spin upward and ''−'' to the spin downward state of the neutron. An α_f profile is recorded within typically 1000 s.

The ^{3}He spin filtering technique is based on the strongly spin-dependent neutron absorption cross section, which is $\sigma_{\uparrow\downarrow} = 3000$ bn for antiparallel and $\sigma_{\uparrow\uparrow} = 5$ bn for parallel neutron states with respect to the ^{3}He polarization. For a given ^{3}He polarization P_{He}, the neutron transmission $T_{\pm}$ of the ^{3}He filter can be written as[13]

$$T_{\pm} = 0.5 \exp\{-\varrho \cdot (1 \mp P_{\mathrm{He}})\}, \tag{1}$$

with the dimensionless opacity $\varrho = 0.073\ \mathrm{bar}^{-1}\,\mathrm{cm}^{-1}\,\text{Å}^{-1} \times p l \lambda$, where l is the length of the ^{3}He cell and p the ^{3}He gas pressure. The associated polarization of the neutrons after passing the ^{3}He cell is then given by

$$p_2 = \frac{T_+ - T_-}{T_+ + T_-}. \tag{2}$$

The ^{3}He spin filter used in this test experiment is a cylindrical cell 100 mm in length and 50 mm in outside diameter (the wall thickness is 5 mm). The cell is fabricated of duran glass with monocrystalline silicon caps of 4 mm thickness (used for beam entry and exit) and filled with polarized ^{3}He gas of pressure $p = 1.45$ bar, resulting in $\varrho = 5.82$.

After filling the cell with polarized ^{3}He the polarization is 55%, but since it decays with a relaxation time $\tau = 60$ h, it drops from 55% to 33% within a typical measuring time of 24 h (see Table I). In order to achieve this long relaxation time, the ^{3}He vessel has to be installed in a homogeneous magnetic environment assuring, as a rule of thumb, a small magnetic field gradient $(1/B)\mathrm{d}B/\mathrm{d}x$ of less than 3×10^{-4} cm^{-1}.[13] In our setup this is realized by a so called Braunbek coil arrangement[32] around the ^{3}He vessel [see Fig. 3(a)]. Figure 3(b) shows the magnetic field inside the Braunbek coils (measured in the presence of the sample magnetization field $B = 400$ mT).

TABLE I. Time-dependence of polarization and transmission parameters of our ^{3}He gas spin filter, calculated for an initial ^{3}He pressure $p = 1.45$ bar and a relaxation time $\tau = 60$ h.

	0 h (%)	24 h (%)	48 h (%)
P_{He}	55	37	25
T_+	3.6	1.3	0.6
T_-	0.0062	0.017	0.0035
p_2	99.7	97.3	89.3

Prior to the actual spin-resolved off-specular scattering experiments the performance of the arrangements was tested carefully (without the sample) and it provided the efficiency of all components acting on the neutron spin. For each experimental condition this has been done following the procedures described in Refs. 33 and 34 which allow a clear-cut determination of the transmission coefficients T_+, T_- of the setup as well as the aforementioned efficiencies of p_1, p_2, f_1, and f_2.

B. Sample preparation

In order to explore the potential of such an experimental setup to detect spin-resolved off-specular neutron scattering,

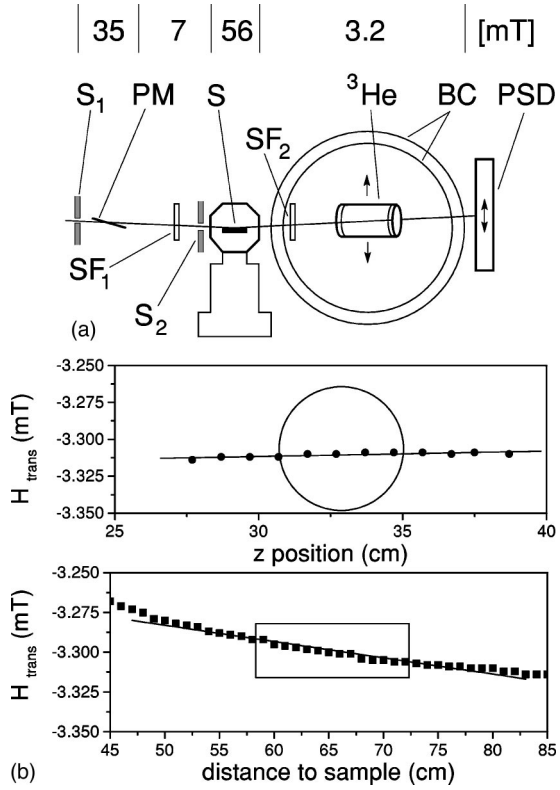

FIG. 3. (a) Magnetic field arrangement around the sample position and the ^{3}He filter. S1 and S2 are the slits defining the angular resolution, here 0.5 mrad. The Mezei flippers are denoted SF_1 and SF_2. PM denotes the transmission mirror and BC the Braunbeck coils. The sample (S), the ^{3}He spin filter (^{3}He), and PSD are also indicated. (b) Measurements of the homogeneity of the transversal fields at the spin filter position as a function of the vertical coordinate (parallel to the surface normal of the sample) and the distance from the sample. The field at sample position is 56 mT. The fields were measured using a Hall probe.

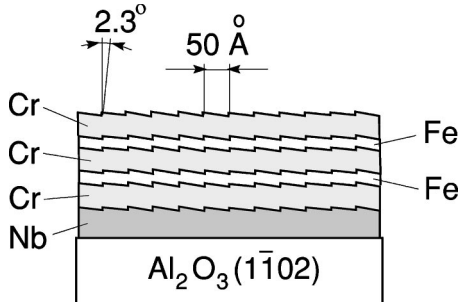

FIG. 4. Schematic view of the sample structure. The terrace structure is due to the growth characteristics of the Nb buffer layer.

we have chosen the model system Fe/Cr, which exhibits biquadratic coupling between adjacent Fe layers.[3,27] A multilayer sample with 200 periods of 19 Å Fe and 42 Å Cr has been grown in the Bochum molecular beam epitaxy (MBE) system at 300 °C in ultrahigh vacuum (better than 10^{-10} mbar) using growth rates of 0.16 Å/s for Cr and 0.2 Å/s for Fe on a Nb buffer (Fig. 4) on an Al_2O_3 $(1\bar{1}02)$ substrate.[35,36] In order to maximize the neutron signal 200 Fe/Cr bilayers were grown on a large 5×5 cm^2 substrate. For protection against oxidation, the sample was covered with a 20 Å Cr layer.[37] Reflection high energy electron diffraction performed during growth indicated a smooth growth front with steps. Energy dispersive x-ray (EDX) analysis gave the relative Fe and Cr concentrations which, combined with the measured superlattice period, provided the layer thicknesses. X-ray scattering and EDX spectra taken from the center and near the edges of the samples confirmed the lateral homogeneity of the sample, obtained by continuous rotation of the sample during growth. The chemical homogeneity determined with a microprobe was better than 1%.

The nature of the Nb/Al_2O_3 $(1\bar{1}02$ epitaxy induces a natural miscut of the Fe/Cr multilayer of $\approx$2.3° which in turn gives rise to a pronounced unidirectional step structure with a high step density and a consequently small lateral step–step distance of $\approx$ 50 Å.[36] Since each Fe/Cr interface may reproduce this step morphology (see Fig. 4), we expect strong off-specular diffuse scattering which should exhibit a pronounced modulation in the z direction (diffuse sheets). The polarized neutron reflectivity of this sample has been studied in detail in the past.[27] A combined neutron reflectivity and high angle neutron scattering study implied a commensurate antiferromagnetic frustrated spiral structure of the Cr which causes the noncollinear average coupling between the Fe layers in this sample.[27] For detailed microscopic understanding of local interlayer coupling the real structure of the multilayer is crucial.

III. EXPERIMENTAL RESULTS

In order to record the off-specular scattering from the Fe/Cr multilayer, the sample was magnetized parallel to the sample surface with a small external field of $B=56$ mT in the easy magnetization direction. This field was maintained during the experiment and defined the quantization direction for the impinging neutrons which was, thus, collinear with the average magnetization of the sample. For each setting of the incidence angle α_i an α_f profile is recorded in the position sensitive detector for all spin combinations $(++, --, +-, -+)$. In this way one obtains spin-resolved off-specular neutron scattering maps in the (α_i, α_f) plane. In this representation of the data the specularly reflected neutrons are displayed along the diagonal line corresponding to $\alpha_i = \alpha_f$ (see also Fig. 2). We have performed the experiment in three modes with increasing spin sensitivity: the unpolarized mode (using an unpolarized neutron beam and no ^{3}He filter) which provides the total off-specular scattering map; the polarized mode (using a polarized neutron beam and no ^{3}He filter) which provides the $(+)$-map and the $(-)$-map; finally, the spin-resolved mode (using a polarized neutron beam with the ^{3}He installed) which provides all four diffuse maps $(++, --, +-, -+)$. In all experiments the incoming neutrons are impinging perpendicular to the miscut-induced terraces of the sample.

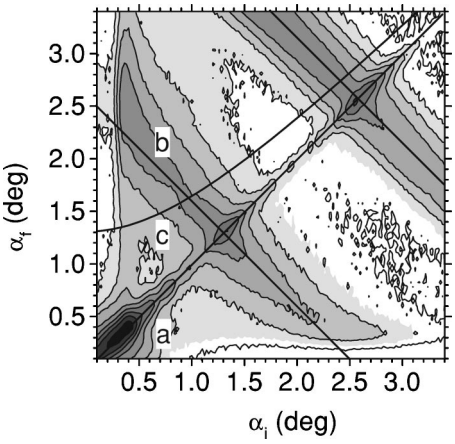

FIG. 5. α_i - α_f map generated from 170 α_i positions. The acquisition time was 650 s. Each point in the intensity map was averaged over 1 mm of the PSD (10 channels) ($\delta\alpha_f=0.044°$). The intensity ranges from 20 to 20 000 counts and the scale is logarithmic. The contour lines are separated by a factor of 2.78.

A. Unpolarized maps

The measured (α_i, α_f) map shown in Fig. 5 discloses a specular intensity along q_z (the $\alpha_i=\alpha_f$ line) and, superimposed, strong diffuse scattering which is strongly bunched into two diffuse sheets perpendicular to the specular rod. The specular intensity essentially consists of three features: the total reflection regime is seen for small angles of incidence, a full-order Bragg reflection from the Fe/Cr double-layer unit cell occurs at $\alpha_i=2.6°$, associated with a perpendicular momentum transfer $q_z=0.104$ Å^{-1}. This periodicity ($L=1$) is mediated by the chemical unit cell and eventually by ferromagnetic coupling present between adjacent Fe layers. The additional Bragg reflection observed at the half-order ($L=0.5$) position is due to doubling of the unit cell caused by antiferromagnetic moments between adjacent Fe layers and is thus purely of magnetic origin. The strongly bunched diffuse sheets emanating from the full-order and the half-order Bragg positions are caused by the miscut-induced roughness of the Fe/Cr interfaces which is apparently strongly correlated in the growth direction. We note that the diffuse scattering is almost constant in the inplane direction (the distor-

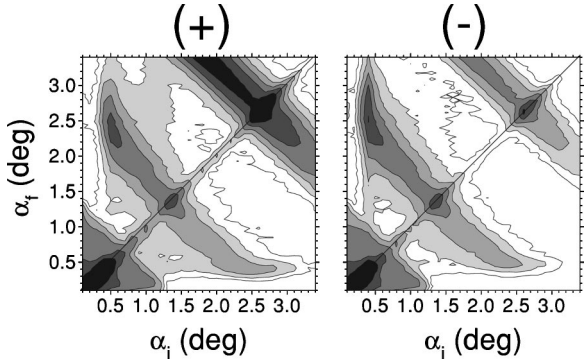

FIG. 6. Same representation as that in Fig. 5, but using polarized neutrons. The image on the left corresponds to $|+\rangle$ neutrons, and the right image to $|-\rangle$ neutrons. The counting time was 2300 s. Intensities are plotted from 60 to 60 000 counts on a logarithmic scale. The contour lines are separated by a factor of 2.36.

tion of the isointensity contours visible at the half-order diffuse sheet is due to Yoneda scattering). This observation can be understood in a straightforward way by the short in-plane length scale of approximately 50 Å which gives rise to this smooth intensity distribution along the half-order and full-order sheet. The noticeable asymmetry in the diffuse intensities in the $q_{\|}$ direction (along the sheets) is caused by the unidirectional step structure of the sample[38] and by the asymmetric resolution function.[39]

B. Polarized maps

The measured polarized contour maps for parallel $(+)$ and antiparallel $(-)$ incident neutron spin are depicted in Fig. 6. On the specular rod, a shift of the critical angle between the $(+)$ and the $(-)$ states is observed, which is indicative of the net magnetization in the sample. In addition, the intensities (both specular and off specular) around the full-order position $(L=1)$ differ by a factor of 4 between the $(+)$ and the $(-)$ maps. Both observations give unambiguous evidence for significant ferromagnetic components in both the average magnetic structure, determined by the vertical arrangement and the magnetic properties of the Fe layers, and the distribution of defects responsible for the diffuse scattering. The simultaneous observation of the antiferromagnetic component (half-order scattering) and the ferromagnetic component implies that the average and local Fe moments in adjacent layers differ in direction and/or magnitude.

C. Spin-resolved maps

The vectorial local spin structures and their spatial correlation inplane and out of plane are unraveled by the four spin-resolved off-specular neutron scattering maps obtained by use of the ^{3}He filter combined with a multidetection system. These maps, which are the primary results of our study, are summarized in Fig. 7. The most apparent effect of the spin analysis is that it subdivides the diffuse maps into two regimes indicated by the dashed lines: for angles α_i and α_f above the dashed lines the off-specular scattering is essentially of a nonspin-flip character, while for smaller angles below these lines the off-specular intensity is dominated by

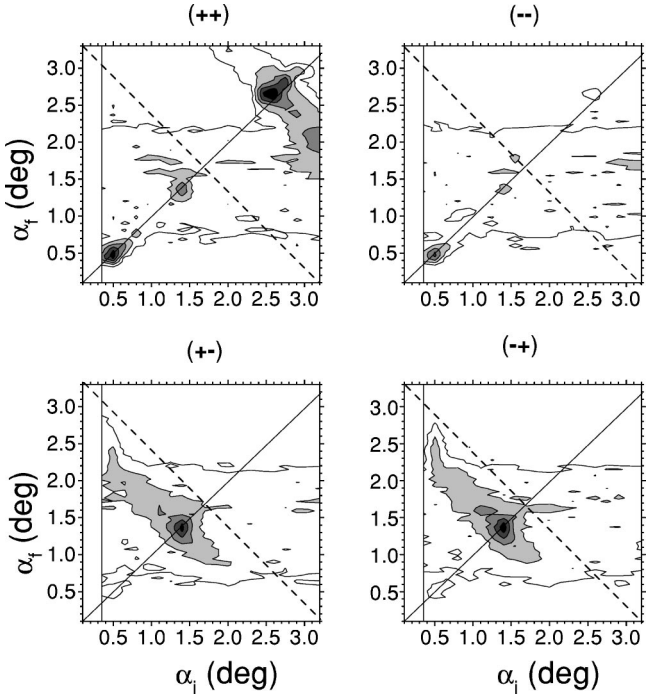

FIG. 7. Four cross sections as a function of the incident and exit angles. The data represent α_f spectra recorded at 20 different α_i positions. The recording time per spectrum was 2200 s. The contour lines range from 100 to 3000 counts on a logarithmic scale and are separated by a factor of 1.53.

spin-flip scattering. The spin-flip nature of the diffuse sheet at the half-order peak gives direct evidence that the local magnetic roughness at the interfaces which is antiferromagnetically correlated between adjacent layers has predominantly perpendicular components with respect to the average magnetization of the multilayer. Interestingly, the spin-resolved maps disclose that all features of the specular rod, in particular their spin-flip and nonspin-flip behavior are identically reproduced in the associated diffuse sheets. Since the spin-flip and nonspin-flip character of the diffuse and the specular intensity is virtually identical, one is forced to conclude that the vertical correlations of the laterally averaged Fe moments and of the local Fe moments are strongly related.

IV. DATA ANALYSIS

The spin-resolved intensity maps presented in Sec. III contain complete information on spin–spin correlations in the multilayer. If we write

$$\langle \underline{s}_i(\underline{r})\underline{s}_j(\underline{r}')\rangle = \langle \underline{s}_i\rangle\langle \underline{s}_j\rangle + (\langle \underline{s}_i(\underline{r})\underline{s}_j(\underline{r}')\rangle - \langle \underline{s}_i\rangle\langle \underline{s}_j\rangle), \quad (3)$$

where $\underline{s}_i(\underline{r})$ and $\underline{s}_j(\underline{r}')$ denote the spin densities at positions $\underline{r}$ and $\underline{r}'$ within layers i and j, respectively, then the first term on the right-hand side is related only to the laterally averaged spin structure that determines the specular reflectivity. The specular reflectivity of the noncollinear spin structure in our Fe/Cr sample has already been discussed in Ref. 27. Here we focus on discussion and theoretical treatment of the diffuse scattering distribution which arises from the second term on the right-hand side of Eq. (3). To that end we extended the supermatrix formalism recently developed for

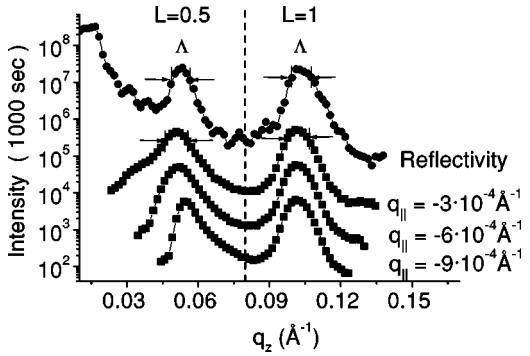

FIG. 8. Pure specular reflectivity (closed circles) and line scans parallel to the specular rod extracted from Fig. 5 [curve type (c)] for different $q_{\|}$ offsets.

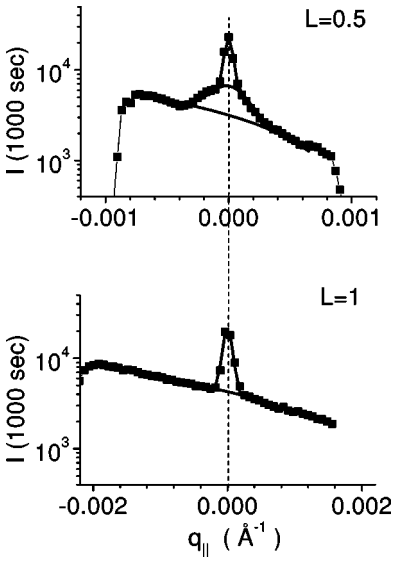

FIG. 9. Line scans along the two diffuse sheets shown in Fig. 5 [curve type (b)] at the half-order position (top) and the full-order position (bottom).

polarized neutron reflectivity[28] to off-specular scattering from arbitrary average spin configurations. An outline of the theory is given in the Appendix.

Before we compare the result of our calculations with the two-dimensional experimental intensity maps, we give direct interpretation of line scans extracted from these maps. Selected line scans provide interesting insights into specific features of the magnetic roughness. In Fig. 5 three such generic scans are indicated as straight lines, denoted a, b, and c.

(1) Scan a (specular scan): This scan measures the lateral average of the nuclear and magnetic scattering length density.
(2) Scan b (diffuse $q_{\|}$ scan): This scan selects the spin–spin correlations within the layers. Such $q_{\|}$ scans have recently been presented and qualitatively discussed.[8]
(3) Scan c (diffuse q_z scan): This type of scan gives access to the local spin correlations between the layers. Such diffuse scans are nowadays standard in x-ray cases,[40] but have so far not been considered in detail in magnetic neutron scattering.

In Fig. 8 we show the measured specular scan and diffuse q_z scans for various values of $q_{\|} = 0.0003$, 0.0006, and 0.0009 Å^{-1}. The vertical dashed line separates the spin-flip (SF) and nonspin-flip (NSF) regimes observed in the spin-resolved measurements. The apparent similarity of the specular and nonspecular peaks is intriguing. Their widths are indicated in Fig. 8 and allow one to determine the length scales over which the average scattering length density as well as local scattering centers at the interfaces are (periodically) correlated: the noticeable width $\Gamma = 0.0842$ Å^{-1} of the specular peaks implies that the vertical correlation length of the layered structure in our multilayer is limited to about $\xi_{\perp} = 2\pi/\Gamma = 750$ Å, i.e., 12 bilayers. This reduced correlation length may originate from growth-related layer thickness variations or from a diffusion-mediated compositional inhomogeneity of the layers due to aging of the sample. Although the lateral homogeneity of the vertically averaged chemical composition and the overall structure (e.g., total thickness) of the multilayer was confirmed using EDX and x-ray scattering (see Sec. II), local sample characteristics may vary laterally within each layer or as a laterally inhomogeneous function of depth. Since all nonspecular peaks display virtually the same widths as the corresponding specular peaks, one is forced to conclude that in particular the vertical correlations of the laterally averaged magnetization and those of the local scattering centers at the rough interfaces are intimately related.

In Fig. 9 we show diffuse $q_{\|}$ scans across $L = 1/2$ and 1. Within the $q_{\|}$ range screened in this feasibility study, we observe a smooth diffuse intensity since we pick up only a small portion of the entire, rather broad diffuse scattering envelope. Note that a peak width of 0.12 Å^{-1} in $q_{\|}$ would be expected for 50 Å correlations which would correspond to the calculated length of the miscut terraces in our sample. In order to determine the width of this broad feature experimentally, the accessible $q_{\|}$ range would need to be properly extended, e.g., by also examining the transmitted beam.[41] A closer inspection of the inplane scans in Fig. 9 reveals a further (larger) length scale in the diffuse scattering across the half-order reflection. This additional scattering is caused by magnetic domains with a typical lateral length scale of 2.5 μm which are antiferromagnetically ordered along the growth direction of the multilayer.

We switch now to discussion of the two-dimensional intensity maps in comparison with model calculations based on the novel supermatrix formalism for off-specular scattering described in the Appendix. The rigorous theoretical treatment of off-specular diffuse scattering has been worked out for x rays in the last decade[42] and is nowadays almost routinely applied to analyze the chemical roughness morphology of thin layers and multilayers.[38] In the case of magnetic roughness studied with neutrons this description becomes considerably more complicated, for example, because of the vector character of the local magnetic-field distribution which imposes a severe challenge to proper theoretical treatment of the spin-dependent scattering cross section and the associated spin-flip processes. A recently presented supermatrix approach[28] allowed us to readily describe the spin-resolved neutron reflectivity from arbitrary, e.g., noncollinear, multilayer structures. The full potential of the spin-

resolved *off-specular* maps presented here, however, can only be exploited when such supermatrix techniques are extended to arbitrary *local* spin structures. This in fact involves a twofold challenge:

(1) the proper theory for local spin–spin correlations associated with magnetic interfacial roughness and magnetic domains within the multilayer and
(2) the development of a convenient spin-dependent off-specular neutron scattering cross section.

In the following we demonstrate that the supermatrix approach for specular reflectivity can be extended to off-specular diffuse scattering. An outline of the theory is given in the Appendix and focuses on the case of strongly conformal roughness. The calculated intensity maps are based on Eqs. (A1)–(A8) in which the lateral roughness structure factor is modeled through a Gaussian, resulting in $S(q_x) = (2\pi)^{3/2}\xi_x \exp(-\frac{1}{2}q_x^2/\xi_x^2)$ after integration over the y direction, i.e., the direction transverse to our position sensitive detector (see Fig. 2). According to our line shape analysis the multilayer exhibits coherent growth of approx 12 Fe/Cr bilayers. For symmetry reasons, we used in our model calculations 16 bilayers of 19 Å Fe and 42 Å Cr, and assumed 90° coupling of two adjacent Fe layers. For simplicity, ideal experimental conditions have been assumed, e.g., an efficiency of 100% for both polarization and spin analysis, as well as magnetically saturated Fe layers (the presence of cap and buffer layers has been neglected in this first approach). For the roughness of all interfaces we used a common value of 4 Å, close to the value determined in Ref. 36, and did not consider eventual systematic variations of the roughness with depth. The results of the calculations are shown in Fig. 10 after resolution correction taking into account the experimental parameters of our experimental setup. As mentioned above, the resolution and illumination corrections result in a asymmetry of the scattered intensity with respect to the specular path. No peculiar correlation function (e.g., like that in Ref. 38) associated with the step distribution was assumed, which would enhance the asymmetry of the scattered intensity with respect to the specular path. The main feature of the experimental result, the spin/flip nature of the half-order sheet, is reproduced by our calculation. However, no additional spin/flip due to local spins misaligned with respect to the mean magnetization of each Fe layer was taken into account. Such ''loose spins'' and lateral or vertical correlations of them would not only lead to additional spin-flip scattering, but also to an interesting magnetic field dependence of the off-specular scattering, which would be different from the behavior of the specular scattering probing the average spin directions. Since it was suggested[43] that loose spins could mediate 90°-type or biquadratic coupling, it would be interesting in the future to calculate their diffuse scattering contributions.

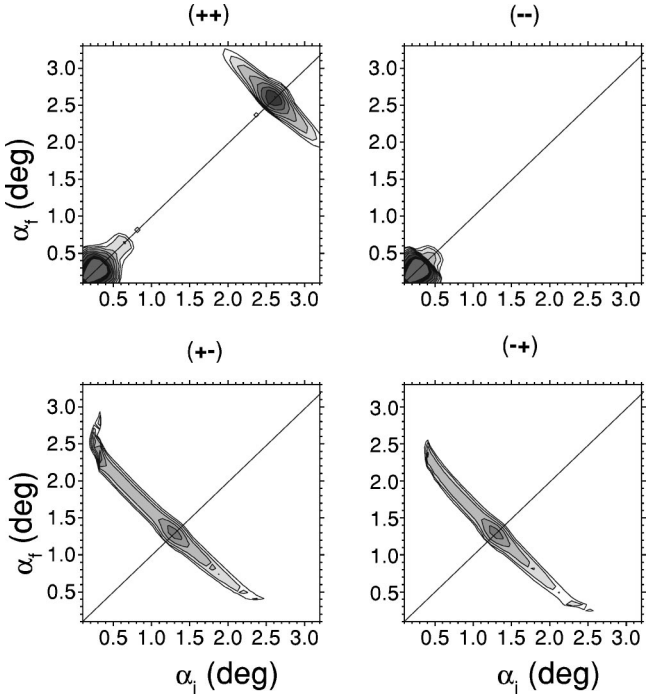

FIG. 10. Model calculation of the NSF (top) and SF (bottom) intensities according to Eq. (A7) for a 16 period Fe/Cr multilayer. The data are plotted on a logarithmic scale, and the contour lines are separated by a factor of 1.53.

V. DISCUSSION

In this work we have focused on experimental aspects and the feasability of spin-resolved off-specular neutron scattering as well as on theoretical aspects. We demonstrated that the combined use of a multidetection system and the polarized ^{3}He gas filtering technique allowed us to obtain spin-resolved off-specular neutron scattering maps from magnetic multilayers which carry detailed information on the spatial distribution of magnetic roughness and magnetic domain structures. Here in Sec. V we will discuss alternatives to our experimental setup and desirable improvements of the theoretical treatment.

The major disadvantage of the ^{3}He spin analysis technique is its low detection efficiency of about 3%. With a conventional setup encompassing a polarizing supermirror, a point detector, and variation of the exit angle, a scan of realistically 15–20 exit angles with statistical quality comparable to that of our line scans could be obtained within the recording time of our PSD spectra. However, even after combining position sensitive detector (PSD) channels in groups of 10, our α_f profiles still contain about five times more data points. The net gain when using a ^{3}He filter instead of a conventional detection scheme is, thus, a factor of 5. Such improved performance is especially desirable for studies of complex multilayers in which data points at many different momentum transfers perpendicular to the surface are needed to characterize the system. In principle, the conventional setup described above could be improved by using the polarizing supermirror in combination with a PSD, rather than a point detector. Serious complications, however, would arise from the fact that the scattered neutrons leave the sample surface under different exit angles and would, thus, hit the polarizing mirror under different angles.

In the discussion of the $q_\parallel$ scans extracted from our data, it has become evident that for samples with a small lateral coherence length a larger range in $q_\parallel$ would be desirable.

With the experimental setup presented here, this can be easily achieved by moving the PSD to negative exit angles, i.e., measuring in transmission geometry. Alternatively, the PSD could be rotated by 90° into the *y* direction (see Fig. 2). This scheme, which is also frequently used in x-ray reflectometry,[4] would provide spin-resolved q_z-q_y maps, instead of the q_z-q_x maps our $\alpha_i-\alpha_f$ maps correspond to. Note, however, that for laterally anisotropic, e.g. stepped, samples like our Fe/Cr multilayer these two maps would not be equivalent. While it might again be possible, although less effective, to use analyzers other than a ^{3}He filter for such an experiment, the unrivaled advantage of ^{3}He filters becomes evident when used in combination with two-dimensional detectors, which would allow one to probe both in-plane directions at the same time. This would improve the efficiency of data collection by another factor of 100 compared to a conventional point-detector scheme. Also, once a ^{3}He filter is filled with polarized helium, it is very convenient to use since it does not require alignment, as opposed to any sophisticated and expensive multimirror arrangement that one might consider as an alternative. For a further comparative discussion of supermirrors and ^{3}He filters we refer to the literature.[44,45]

It can be concluded that ^{3}He filters, especially when used in connection with two-dimensional detectors, will provide a promising tool for the investigation of advanced magnetic materials. It is expected that such two-dimensional detection schemes as those recently used for SANS[24] will be available for polarized neutron reflectometry in the near future. Moreover, an improvement of the ^{3}He polarization from the current 55% to 70% is envisaged,[25,26] and this would, in our case, improve the degree of polarization by roughly a factor of 3 and, more important, the transmission from the current 3% to as much as 9%–10%.

With regard to the analysis of our spin-resolved diffuse intensity maps in light of magnetic roughness, we demonstrated that simple assumptions about the average spin structure in the multilayer, about the magnetic scattering potential at the interfaces and about the roughness correlations between the interfaces can already explain the gross features of off-specular scattering observed. Theoretical treatment of our data can easily be refined, both in some general and sample-related aspects: The effect of roughness can be included by subdividing the interfaces into slabs. Arbitrary roughness correlations between the interfaces can be modeled via $K_{nn'}$ in Eq. (A2). An increase of the interface roughness from the substrate to the surface can be introduced, the presence of which was indicated by a comparison of our neutron and x-ray reflectivity data. Specific spin configurations and resulting scattering potentials at the interfaces can be tested. However, due to the arguments given in the following two paragraphs, we deliberately restricted the analysis to the simplest treatment possible, on the one hand, in order to keep the computation times within a reasonable range and, on the other hand, in order not to overinterpret the still relatively limited data obtained from our highly complex sample.

One has to emphasize that, compared to diffuse x-ray scattering from multilayers, the corresponding computations for the polarized neutron case are considerably more involved. In the neutron case, one has to account for birefringence, for both nuclear and a magnetic scattering contrast and the corresponding interface–interface correlations, and, in semiclassical terms, for changes of the orientation of the neutron magnetic moment as the neutron waves propagate through the multilayer (precession), unless the magnetizations of all the layers are collinear with the neutron polarization. Note also that a simplified kinematic approach, as is frequently used for x-ray scattering (see, e.g., Ref. 38), would entirely neglect most of these effects and, thus, inherently not be able to provide correct information about the magnetic structure of the sample. Using a numerically more involved dynamic matrix formalism was therefore fundamental to calculating the spin-resolved off-specular scattering from our sample.

In order to obtain pronounced off-specular diffuse scattering for this feasibility study, we chose a relatively complicated multilayer sample that exhibited a large number of Fe/Cr bilayers, a noncollinear spin structure, and a high, presumably depth-dependent interface roughness induced by a growth-related miscut. While these sample properties tend to complicate data analysis, they in fact provided us with the desired high diffuse scattering intensities. Note that, although the high degree of polarization obtained with our ^{3}He spin filter was associated with a low transmission, it was desirable for this first study in order to clearly discriminate between nonspin-flip and spin-flip intensities. With the expected improvements of future ^{3}He gas spin filters, similar studies on simpler samples with a smaller relative amount of diffuse scattering should become feasible in which further details of interface morphologies can be revealed.

Having understood the gross features of our intensity maps, we are now working on finalizing the data analysis based on the recently developed supermatrix approach. This approach provides a convenient and efficient analytical tool with which to handle the complexity of such spin-resolved diffuse scattering intensities from arbitrary spin structures. The first model calculations presented here clearly indicate its future potential. We envisage that a supermatrix software code for analyzing such off-specular intensity maps will be available shortly on our homepage.[46]

ACKNOWLEDGMENTS

The authors thank Thomas Krist, Hahn-Meitner-Institut (Berlin, Germany), who kindly provided the polarizing supermirrors. The support of the management and staff at the Intitute Laue–Langevin is gratefully acknowledged. The work was funded by the Bundesministerium für Bildung und Forschung, Berlin, Germany under Contract No. 03-DO5MPG.

APPENDIX: OUTLINE OF THE SUPERMATRIX APPROACH TO OFF-SPECULAR SCATTERING

The total cross section for neutron reflection and diffuse scattering from a multilayer is[42]

$$\sigma_{\mathrm{tot}}=\overline{A}\mathcal{R}(\mathbf{k}_i)+\int_{\Delta\Omega_f}\frac{\mathrm{d}\sigma}{\mathrm{d}\Omega}(\mathbf{k}_i,\mathbf{k}_f)\mathrm{d}\Omega_f, \tag{A1}$$

where $\mathcal{R}(\mathbf{k}_i)$ is the polarized neutron reflectivity, $\overline{A}$ is the cross section of the detected portion of the reflected beam, $d\sigma/d\Omega$ is the differential cross section for diffuse scattering of polarized neutrons, and $\Delta\Omega_f$ is the solid angle subtended by the detector. The formalism developed in this Appendix is proposed as a tool to quantitatively interpret off-specular scattering intensities from a magnetic multilayer in a spin-resolved neutron experiment. Since the neutron optics are treated according to dynamical scattering theory, the formalism is applicable even for highly perfect multilayers.

We focus in what follows on the differential diffuse scattering cross section from a multilayer with small roughness. Then $d\sigma/d\Omega$ can be represented in the form[38]

$$\frac{d\sigma}{d\Omega}=\frac{Ak_0^4}{16\pi^2}\sum_{n,n'=1}^{N}K_{nn'}C_nC_{n'}^*, \tag{A2}$$

where A is the illuminated surface area, k_0 the wave number of the incident neutrons, and C_n are the scattering amplitudes associated with the rough interfaces $n=1,\ldots,N$. The coefficients $K_{nn'}$ are determined by the roughness correlations among the interfaces. For simplifying the treatment here, we assume that all interfaces have the same lateral morphology, described by a structure factor $S(\mathbf{q}_{||})$ [normalized to $(2\pi)^2$]. Then $K_{nn'}=\delta_{nn'}S(\mathbf{q}_{||})$ holds for vertically uncorrelated interfaces and $K_{nn'}=1\cdot S(\mathbf{q}_{||})$ in the case of perfect vertical correlations (ideal conformal roughness).[38,47] Since our observation indicates a highly correlated roughness morphology (diffuse Bragg sheets), we restrict our considerations here to the latter case, thus obtaining

$$\frac{d\sigma}{d\Omega}=(Ak_0^4/16\pi^2)\left|\sum_{n=1}^{N}C_n\right|^2S(\mathbf{q}_{||}). \tag{A3}$$

Within the distorted wave Born approximation (DWBA), the matrix elements C_n are given by[47]

$$C_n=\int_{z_n}^{\infty}\langle\psi^f(z)|\hat{V}_n(z)|\psi^i(z)\rangle dz + \int_{-\infty}^{z_n}\langle\psi^f(z)|-\hat{V}_n(z)|\psi^i(z)\rangle dz, \tag{A4}$$

where $|\psi^{i,f}\rangle$ denote the initial and final neutron (spin or) wave function for the ideal system without roughness, and $\pm\hat{V}_n(z)$ is the susceptibility contrast (or scattering potential) arising from the root mean square (rms) roughness σ_n of interface n, located a distance z_n from the surface. As usual, we model the scattering potential by the error function in the form

$$\hat{V}_n(z)=\frac{1}{2}\left\{1+\mathrm{erf}\left(-\frac{|z-z_n|}{\sqrt{2}\sigma_n}\right)\right\}\Delta\hat{V}_n, \tag{A5}$$

with $\Delta\hat{V}_n=(4\pi/k_0^2)(\hat{N}_{n-1}-\hat{N}_n)$ as the scattering potential. Following the approach presented in Ref. 28, we define the operators $\hat{N}$ in terms of their eigenvalues and the vector $\hat{\boldsymbol{\sigma}}$ of Pauli matrices and write $\hat{N}_n=N_n^{\mathrm{nuc}}+N_n^{\mathrm{mag}}\mathbf{b}_n\hat{\boldsymbol{\sigma}}$ with $N_n^{\mathrm{nuc,mag}}$ denoting the nuclear and magnetic scattering length densities in layer n, and $\mathbf{b}_n$ the unit vector along the respective magnetic field. For $\sigma_n q_z^n, \sigma_n q_z^{n-1}\ll 1$, with q_z^n as the z component of the momentum transfer within layer n, it can be shown [by evaluating the integrals in Eq. (A4)] that

$$C_n\approx(2/\pi)^{1/2}\sigma_n\langle\psi_n^f|\Delta\hat{V}_n|\psi_n^i\rangle. \tag{A6}$$

The neutron states $|\psi_n^{i,f}\rangle=|\psi^{i,f}(z_n)\rangle$ can be calculated using the supermatrix formalism developed in Ref. 28. If the polarization states of the incident and scattered beam at the surface, defined by the polarizer and analyzer characteristics, are denoted $|\chi^{i,f}\rangle$, and if $\hat{\rho}^{i,f}$ are the corresponding density matrices, then, after straightforward but somewhat lengthy mathematics, one finally arrives at

$$\sum_{n=1}^{N}C_n=\langle\chi^f|(1+\tilde{R}^{fT},\quad i|p^f|\{1-\tilde{R}^{fT}\}) \times\tilde{W}\begin{pmatrix}1+\tilde{R}^i\\ ip^i\{1-\tilde{R}^i\}\end{pmatrix}|\chi^i\rangle, \tag{A7}$$

or, in terms of the density matrices $\rho^{i,f}$,

$$\overline{\left|\sum_{n=1}^{N}C_n\right|^2}=\mathrm{Tr}\left\{\hat{\rho}^+(1+\tilde{R}^{fT},i|p^f|\{1-\tilde{R}^{fT}\}) \times\tilde{W}\begin{pmatrix}1+\tilde{R}^i\\ ip^i\{1-\tilde{R}^i\}\end{pmatrix}\hat{\rho}_0(1+\tilde{R}^{i+},\quad ip^i\{1-\tilde{R}^{i+}\}) \times\tilde{W}^+\begin{pmatrix}1+\tilde{R}^{f*}\\ i|p^f|\{1-\tilde{R}^{f*}\}\end{pmatrix}\right\}. \tag{A8}$$

Here $\tilde{W}$ is

$$\tilde{W}=\sum_{n=1}^{N}\tilde{S}_1^{fT}\cdot\ldots\cdot\tilde{S}_n^{fT}\begin{pmatrix}(2/\pi)^{1/2}\sigma_n\Delta\hat{V}_n & 0\\ 0 & 0\end{pmatrix}\tilde{S}_n^i\cdot\ldots\cdot\tilde{S}_1^i, \tag{A9}$$

where $\tilde{S}^{i,f}=\tilde{S}(|p^{i,f}|)$ are the transfer supermatrices,[28] $\tilde{R}^{i,f}=\tilde{R}(|p^{i,f}|)$ are the reflectance matrices, and $p^{i,f}$ are the vacuum wave numbers perpendicular to the surface.

In the scalar case (x-ray case), and for a simple semi-infinite substrate, the right-hand side of Eq. (A8) may be reduced to $|\tilde{T}^f\tilde{W}\tilde{T}^i|^2$ with the transmission coefficients $\tilde{T}=1+\tilde{R}$. Then, the scattering cross section in Eq. (A2) becomes

$$\frac{d\sigma}{d\Omega}=\frac{Ak_0^4\sigma_0^2}{(2\pi)^3}|\tilde{T}^f\Delta\hat{V}_0\tilde{T}^i|^2S(\mathbf{q}_{||}), \tag{A10}$$

which is consistent with the well-known expression for grazing-angle scattering as given, e.g., in Ref. 47.

[1] A. Fert, P. Grünberg, A. Barthelemy, F. Petroff, and W. Zinn, J. Magn. Magn. Mater. **140**, 1 (1995).
[2] J. F. Ankner and G. P. Felcher, J. Magn. Magn. Mater. **200**, 741 (1999).
[3] D. T. Pierce, J. Unguris, R. J. Celotta, and M. D. Stiles, J. Magn. Magn. Mater. **200**, 290 (1999).
[4] V. Holy and T. Baumbach, Phys. Rev. B **49**, 10668 (1994).

[5] J. F. MacKay, C. Teichert, D. E. Savage, and M. G. Lagally, Phys. Rev. Lett. **77**, 3925 (1996).
[6] R. M. Osgood III, S. K. Sinha, J. W. Freeland, Y. U. Idzerda, and S. D. Bader, J. Magn. Magn. Mater. **198–199**, 698 (1999).
[7] C. S. Nelson, G. Srajer, J. C. Lang, C. T. Venkataraman, S. K. Sinha, H. Hashizume, N. Ishimatsu, and N. Hosoito, Phys. Rev. B **60**, 12234 (1999).
[8] J. A. Borchers *et al.*, Phys. Rev. Lett. **82**, 2796 (1999).
[9] F. Tasset, Physica B **174**, 506 (1991), and references therein.
[10] W. J. Cummings, O. Häusser, W. Lorenzon, D. R. Svenson, and B. Larson, Phys. Rev. A **51**, 4842 (1995), and references therein.
[11] R. Surkau *et al.*, Nucl. Instrum. Methods Phys. Res. A **384**, 444 (1997).
[12] J. Kulda, A. Wildes, A. Martin-Martin, W. Müller, W. Heil, H. Humblot, and F. Tasset, Physica B **241**, 136 (1997).
[13] W. Heil, K. Andersen, D. Hofmann, H. Humblot, J. Kulda, E. Lelievre-Berna, O. Schärpf, and F. Tasset, Physica B **241–243**, 56 (1998).
[14] W. Heil, J. Dreyer, D. Hofmann, H. Humblot, E. Lelievre-Berna, and F. Tasset, Physica B **268**, 328 (1999).
[15] A. Danzig and A. Rupp, Physica B **268**, 344 (1999).
[16] G. L. Jones, T. R. Gentile, A. K. Thompson, Z. Chowdhuri, M. S. Dewey, W. M. Snow, and F. E. Wietfeldt, Nucl. Instrum. Methods Phys. Res. A **440**, 772 (2000).
[17] J. Dreyer, L. P. Regnault, E. Bourgeat-Lami, E. Lelievre-Berna, S. Pujol, F. Thomas, M. Thomas, and F. Tasset, Nucl. Instrum. Methods Phys. Res. A **449**, 638 (2000).
[18] J. Kulda *et al.*, Physica B **268**, 252 (1999).
[19] W. Heil *et al.*, Physica B **268**, 289 (1999).
[20] M. Acet, W. F. Wassermann, K. H. Andersen, J. Kulda, A. P. Murani, and A. Wildes, Physica B **276**, 728 (2000).
[21] O. Zimmer, T. M. Müller, P. Hautle, W. Heil, and H. Humblot, Phys. Lett. B **455**, 62 (1999).
[22] W. G. Williams, Nucl. Instrum. Methods Phys. Res. A **428**, 446 (1999).
[23] J. Becker *et al.*, Nucl. Instrum. Methods Phys. Res. A **402**, 327 (1998).
[24] T. R. Gentile, G. L. Jones, A. K. Thompson, J. Barker, C. J. Glinka, B. Hammouda, and J. W. Lynn, J. Appl. Crystallogr. **33**, 771 (2000).
[25] W. Heil (private communication).
[26] E. Lelievre-Berna and F. Tasset, Physica B **268**, 21 (1999).
[27] A. Schreyer, C. F. Majkrzak, Th. Zeidler, T. Schmitte, P. Bödeker, K. Theis-Bröhl, A. Abromeit, J. Dura, and T. Watanabe, Phys. Rev. Lett. **79**, 4914 (1997); A. Schreyer, J. F. Ankner, Th. Zeidler, H. Zabel, M. Schäfer, J. A. Wolf, P. Grünberg, and C. F. Majkrzak, Phys. Rev. B **52**, 16066 (1995).
[28] A. Rühm, B. P. Toperverg, and H. Dosch, Phys. Rev. B **60**, 16073 (1999).
[29] H. Dosch, K. Al Usta, A. Lied, W. Drexel, and J. Peisl, Rev. Sci. Instrum. **63**, 5533 (1992).
[30] R. Günther, W. Donner, B. P. Toperverg, and H. Dosch, Phys. Rev. Lett. **81**, 116 (1998).
[31] B. Toperverg, A. Vorobyev, G. Gordeyev, B. Nickel, W. Donner, H. Dosch, and Th. Rekveldt, Physica B **283**, 203 (2000).
[32] W. Braunbek, Z. Phys. **88**, 399 (1934); R. S. Caprari, Meas. Sci. Technol. **6**, 593 (1995).
[33] W. G. Williams, *Polarized Neutrons* (Clarendon, Oxford, 1988).
[34] A. R. Wildes, Rev. Sci. Instrum. **70**, 4241 (1999).
[35] S. M. Durbin, J. A. Cunningham, M. E. Mochel, and C. P. Flynn, J. Phys. F: Met. Phys. **11**, L223 (1981); **12**, L75 (1982); **15**, L221 (1985).
[36] K. Theis-Bröhl, I. Zoller, P. Bödeker, H. Zabel, L. Brendel, M. Belzer, and D. E. Wolf, Phys. Rev. B **57**, 4747 (1998).
[37] A. Stierle and H. Zabel, Europhys. Lett. **37**, 365 (1997).
[38] E. A. Kondrashkina, E. A. Kondrashkina, S. A. Stepanov, R. Opitz, M. Schmidbauer, R. Köhler, R. Hey, M. Wassermeier, and D. V. Novikov, Phys. Rev. B **56**, 10469 (1997).
[39] A. Gibaud, G. Vignaud, and S. K. Sinha, Acta Crystallogr., Sect. A: Found. Crystallogr. **49**, 642 (1993).
[40] See, for example, V. Holy *et al.*, *High-Resolution X-Ray Scattering from Thin Films and Multilayers*, Springer Tracts in Modern Physics (Springer, Heidelberg, 1999), Vol. 149.
[41] C. Munster, T. Salditt, M. Vogel, R. Siebrecht, and J. Peisl, Europhys. Lett. **46**, 486 (1999).
[42] S. K. Sinha, E. B. Sirota, S. Garoff, and H. B. Stanley, Phys. Rev. B **38**, 2297 (1988).
[43] J. C. Slonczewski, J. Appl. Phys. **73**, 5957 (1993).
[44] O. Zimmer *et al.*, Nucl. Instrum. Methods Phys. Res. A **440**, 764 (2000).
[45] L. D. Cussen, D. J. Goossens, and T. J. Hicks, Nucl. Instrum. Methods Phys. Res. A **440**, 409 (2000).
[46] http://wwwmf.mpi-stuttgart.mpg.de/abteilungen/dosch/dosch.html
[47] S. Dietrich and A. Haase, Phys. Rev. **260**, 1 (1995).